Optimal single-port matching impedance for capacity maximization in compact MIMO arrays

Fei, Yuanyuan; Fan, Yijia; Lau, Buon Kiong; Thompson, John S.

Published in:
IEEE Transactions on Antennas and Propagation

DOI:
10.1109/TAP.2008.2005463

2008

Document Version:
Peer reviewed version (aka post-print)

Optimal Single-Port Matching Impedance for Capacity Maximization in Compact MIMO Arrays

Yuanyuan Fei, Yijia Fan, Buon Kiong Lau, John S. Thompson

Abstract

A complete MIMO system model with compact arrays at both link ends containing arbitrary matching networks is presented based on a Z-parameter approach. The complete channel matrix including the coupling effect is also presented. Utilizing this system model, the optimum single-port matching impedance for capacity maximization is derived for a 2×2 MIMO system with coupling at the receivers only. A closed-form result for the optimum matching impedance in high signal-to-noise ratio scenarios is given and proved to be equal to the input impedance of the receive end. Simulation of ideal dipoles verifies our analytical results and demonstrates the superiority of the optimum matching to other matching conditions in improving MIMO system performance. Experimental data for monopoles is also presented to further confirm our numerical findings and validate the accuracy of our derivation.

I. Introduction

A. Background

The comprehensively studied multiple-input multiple-output (MIMO) systems promise significant gains in spectrum efficiency and link reliability by deploying multiple antennas at both ends

Part of this work has been accepted for the IEEE Global Telecommunications Conference, Washington D.C., USA, Nov. 2007.

Y. Fei and J. S. Thompson are with the Institute for Digital Communications, Joint Research Institute for Signal & Image Processing, School of Engineering & Electronics, the University of Edinburgh, Edinburgh, EH9 3JL, UK (email: y.fei@ed.ac.uk, john.thompson@ed.ac.uk).

Y. Fan is with the Department of Electrical Engineering, Princeton University, Princeton, NJ, 08544, USA (e-mail: yijiafan@princeton.edu).

B. K. Lau is with the Department of Electrical and Information Technology, Lund University, SE-221 00 Lund, Sweden (e-mail: bklau@ieee.org).

of a wireless link [1]–[3]. An $N \times N$ MIMO system can achieve N times capacity benefit over the single-input single-output (SISO) if operating in an independent and identically-distributed (i.i.d.) channel [4]. However, the i.i.d. channel may not be achieved in practice due to insufficient antenna separation or non-uniformly distributed scatterers in the non-line-of-sight (NLOS) environment. In particular, the integration of multiple antennas into the subscriber end is affected by the limited design volume, which results in significant system performance degradation [2], [5], [6].

In narrowband MIMO systems, it is widely agreed that mutual coupling (MC) which becomes significant for small antenna spacing can reduce the signal correlation by distorting the radiation patterns of each element [7]–[9]. However, it will also induce a mismatch between the characteristic impedance of the circuit and the antenna input, which is detrimental to the capacity performance [10]. This conflicting outcome of the MC effect is one important factor which contributes to different conclusions of its impact on MIMO capacity performance [8], [11]–[19].

Two methods in *n*-port theory are usually used to study compact MIMO systems. One is S-parameter analysis [9], [16], [17] which reflects the wave transmission in an *n*-port electrical network; the other is Z-parameter analysis [10]–[12], [20] which expresses the voltage and current relations among all ports. Various matching networks can be introduced [16] to improve the MIMO capacity performance, while more varieties of matching networks are examined in [21]. It is proved in [9], [16] that the so-called *multiport-conjugate match* (MCM) can realize zero output correlation, lossless power transfer from the antennas to the loads for any antenna spacing, and offer significant capacity improvement for very small antenna spacings. Nevertheless, the optimum MCM can only be achieved for a small bandwidth [22] in wideband systems. Apart from that, the MCM is not easy to implement as it involves multiple circuit components interconnected across the antenna ports [23]. Instead, the *single-port match* (SPM) [10], [20]–[22] is a practical, if suboptimal solution, as it provides capacity improvement compared to the non-matched case and has a broader bandwidth than the MCM.

B. Contributions of the paper

We develop a complete framework study for $N \times N$ MIMO systems including the MC effect at both link ends using Z-parameters, which is suitable for any kind of single-mode antennas at the link ends with any matching networks. The framework is applicable to any propagation channels. Then we simplify the model and show that the MIMO system studied in [10], [20] is

a special case of our model.

We state the derivation of the optimum SPM for capacity maximization of a 2×2 MIMO system using an upper bound of the MIMO ergodic capacity. The deviation holds for all single-mode antennas. Furthermore, the closed-form result of the optimum SPM for capacity maximization in high signal-to-noise ratio (SNR) scenarios is also delivered and proved to be the *input impedance* of the receive antennas.

We illustrate the above derivation using ideal dipole antennas. A perfect match is shown between analytical and simulation results. Moreover, we present the advantage of using the optimum SPM compared to other SPM cases for MIMO system performance. To demonstrate the practical value of our analytical study, an *experimental* monopole array is designed for MIMO capacity evaluation, which further confirms our findings in previous contributions.

C. Relation between previous and current work

Received power maximization or zero output correlation can be achieved by selecting proper SPM [24] for very close antenna spacing ($d = 0.05\lambda$), which has been confirmed by the experimental implementation in [25]. However, it is observed in [20] that the optimum SPM to maximize the capacity is different from the solutions that either maximize the received power or achieve zero correlation. The analytical derivation of the optimum SPM for the capacity maximization is delivered in this work.

The Z-parameter network presented in this paper is an improvement of the previous work [10]–[12], [20]. In [11], the system model is approximated for multiple antennas of a fixed length at the receiver and ignores the effect of matching networks. Although compact MIMO receivers with various matching impedances are examined in [10], [20], no complete Z-parameter framework analysis and analytical result for the optimal SPM are given. The author in [12] did present a Z-parameter MIMO system but with an inappropriate channel matrix expression, which will be further discussed in Section II, and no matching network was included in the study.

Practical amplifier noise models have recently been used to study the impact of matching networks on diversity [26] and MIMO capacity [27], [28] performance. The minimum noise figure match is claimed to be an optimal solution which can outperform the MCM. However, similar to the MCM, multiport matching networks are need to achieve the minimum noise figure

performance. In this paper, we limit our study of SPM to the simple 'receiver noise model' provided in [16].

The remainder of this paper is organized as follows. Section II presents the analysis framework of the MIMO system model using Z-parameters. Section III provides the numerical deviation of the optimum SPM for a 2×2 MIMO system, and gives closed-form results in high SNR regime. Section IV applies the analytical results in Section III to ideal dipole antennas, and compares with the simulation results. The superiority of the optimum SPM for compact MIMO arrays to other matching conditions is also discussed. Results for experimental monopole antennas are provided in Section V to support our analytical studies. Conclusions are given in Section VI.

In this paper, the superscripts ^{T}, *, and ^{H} represent matrix transpose, complex conjugate, and conjugate transpose operators, respectively. $\mathbf{I}_N$ denotes the $N \times N$ identity matrix. The notations Tr($\mathbf{A}$), $E\{\mathbf{A}\}$, det($\mathbf{A}$) and $(\mathbf{A})_{ij}$ denote the trace, expectation, determinant and the (i,j)-th element of the matrix $\mathbf{A}$, respectively. The notation $\mathrm{Re}\{\cdot\}$ is used to denote the real part of a complex number/matrix and vec$(\cdot)$ is the columnwise vectorization operation of a matrix.

II. MIMO System Analysis Based on Z-Parameters

A narrowband $N \times N$ MIMO system is considered. For simplicity we assume that the channel is frequency-flat, rich scattering, and without a line-of-sight (LOS) propagation component. Also it is assumed that the transmitter and receiver arrays are linear, the array elements are of identical polarization, the dimension of the arrays is negligible compared to the link distance, and initially the array elements of both ends are separated by over half-a-wavelength.

According to the *n*-port theory, the channel transfer function between the transmit and the receive arrays in Fig. 1 can be represented as [12]

$$\begin{bmatrix} \mathbf{v}_T \\ \mathbf{v}_R \end{bmatrix} = \begin{bmatrix} \mathbf{Z}_{TT} & \mathbf{Z}_{TR} \\ \mathbf{Z}_{RT} & \mathbf{Z}_{RR} \end{bmatrix} \begin{bmatrix} \mathbf{i}_T \\ \mathbf{i}_R \end{bmatrix} \tag{1}$$

where $\mathbf{v}_T = [V_{T1}, V_{T2}, ..., V_{TN}]^T$, $\mathbf{i}_T = [I_{T1}, I_{T2}, ..., I_{TN}]^T$ are the voltage and current vectors at the transmitter, respectively. Similarly, $\mathbf{v}_R = [V_{R1}, V_{R2}, ..., V_{RN}]^T$, $\mathbf{i}_R = [I_{R1}, I_{R2}, ..., I_{RN}]^T$ denote the voltages and currents at the receiver. The $N \times N$ matrices $\mathbf{Z}_{TT}$ and $\mathbf{Z}_{RR}$ are antenna impedance matrices containing the self and mutual impedances of the transmitter and receiver, respectively. The matrix $\mathbf{Z}_{RT}$ can be translated as the trans-impedance matrix [16] due to the

impact of transmit end currents on the receive end voltages. We define $\mathbf{Z}_{TR} = 0$ to indicate that the transmitters are blind to the conditions (or currents) at the receivers.

The transmit antennas are usually assumed to be spaced sufficiently far apart, but even then mismatches between antennas and corresponding sources still exists. As future wireless communication may involve peer-to-peer transmission between compact MIMO terminals (eg. mobile cooperation [29]), MC will be an issue for both link ends. Thus, a source impedance network $\mathbf{Z}_S$ is inserted between the sources and transmit antennas in Fig. 1 to ensure an efficient power transmission. The relation between the source voltage $\mathbf{v}_S$ and transmit voltage $\mathbf{v}_T$ is

$$\mathbf{v}_T = \mathbf{Z}_{TT}\mathbf{i}_T = \mathbf{Z}_{TT}\left(\mathbf{Z}_{TT} + \mathbf{Z}_S\right)^{-1}\mathbf{v}_S \tag{2}$$

where $\mathbf{v}_S = [V_{S1}, V_{S2}, ..., V_{SN}]^T$. Also the total average transmitted power is

$$P_T = E\left\{\mathrm{Tr}\left(\mathrm{Re}\left\{\mathbf{Z}_{TT}\mathbf{i}_T\mathbf{i}_T^H\right\}\right)\right\} = E\left\{\mathrm{Tr}\left(\mathbf{R}_T^{1/2}\mathbf{Z}_{T+S}^{-1}\mathbf{v}_S\mathbf{v}_S^H\mathbf{Z}_{T+S}^{-H}\mathbf{R}_T^{1/2(H)}\right)\right\} \tag{3}$$

where $\mathbf{R}_T = \mathrm{Re}\left\{\mathbf{Z}_{TT}\right\}$ and $\mathbf{Z}_{T+S} = \mathbf{Z}_{TT} + \mathbf{Z}_S$.

In the compact receive subsystem of Fig. 1, an impedance matching network $\mathbf{Z}_L$ is added after the receive antennas to compensate for the MC induced power reduction. Utilizing circuit theory at the receive subsystem it is easy to obtain

$$\mathbf{v}_R = -\mathbf{Z}_L\mathbf{i}_R. \tag{4}$$

Substituting (4) into (1) we find the receive voltage $\mathbf{v}_R$ as a function of the transmit voltage $\mathbf{v}_T$

$$\mathbf{v}_R = \left(\mathbf{I}_N + \mathbf{Z}_{RR}\mathbf{Z}_L^{-1}\right)^{-1}\mathbf{Z}_{RT}\mathbf{Z}_{TT}^{-1}\mathbf{v}_T = \overbrace{\underbrace{\mathbf{Z}_L\left(\mathbf{Z}_L + \mathbf{Z}_{RR}\right)^{-1}\mathbf{Z}_{RT}\left(\mathbf{Z}_{TT} + \mathbf{Z}_S\right)^{-1}}_{-\mathbf{i}_R}\mathbf{v}_S}^{\mathbf{H}_V} \tag{5}$$

where $\mathbf{Z}_{L+R} = \mathbf{Z}_L + \mathbf{Z}_{RR}$ and $\mathbf{H}_V$ is the channel/voltage transfer matrix [12]. However, because only the voltage across the resistance can be exploited by the receiver, $\mathbf{H}_V$ has to be modified to fulfill the power transfer requirement. We substitute $\mathbf{i}_R$ as defined in (5), then the total average received power of the MIMO system can be represented as

$$\begin{aligned} P_R &= E\left\{\mathrm{Tr}\left(\mathrm{Re}\left\{\mathbf{Z}_L\mathbf{i}_R\mathbf{i}_R^H\right\}\right)\right\} \\ &= E\left\{\mathrm{Tr}\left(\mathbf{R}_L^{1/2}\mathbf{Z}_{L+R}^{-1}\mathbf{Z}_{RT}\mathbf{Z}_{T+S}^{-1}\mathbf{v}_S\mathbf{v}_S^H\mathbf{Z}_{T+S}^{-H}\mathbf{Z}_{RT}^H\mathbf{Z}_{L+R}^{-H}\mathbf{R}_L^{1/2(H)}\right)\right\} \end{aligned} \tag{6}$$

where $\mathbf{R}_L = \mathrm{Re}\{\mathbf{Z}_L\}$. If only the receiver knows the channel conditions, P_T can be evenly distributed across the antennas at the transmit end. Then (6) becomes

$$P_R = E\left\{\mathrm{Tr}\left(\mathbf{H}_{mc}\frac{P_T}{N}\mathbf{I}_N\mathbf{H}_{mc}^H\right)\right\} \tag{7}$$

where $\mathbf{H}_{mc}$ is the channel transfer matrix between the source and the receiver load including the MC effect as represented in Fig. 1. Equation (3) can be substituted into (7) to give

$$P_R = \frac{1}{N}E\left\{\mathrm{Tr}\left(\mathbf{H}_{mc}\mathbf{R}_T^{1/2}\mathbf{Z}_{T+S}^{-1}\mathbf{v}_S\mathbf{v}_S^H\mathbf{Z}_{T+S}^{-H}\mathbf{R}_T^{(1/2)(H)}\mathbf{H}_{mc}^H\right)\right\}. \tag{8}$$

Comparing (6) and (8) we have

$$\mathbf{H}_{mc} = \mathbf{R}_L^{1/2}\mathbf{Z}_{L+R}^{-1}\mathbf{Z}_{RT}\mathbf{R}_T^{-1/2} = \mathbf{R}_L^{1/2}\mathbf{Z}_{L+R}^{-1}\mathbf{H}\mathbf{R}_T^{-1/2}. \tag{9}$$

where the channel $\mathbf{H}$ can be any physical or statistical propagation model which properly reflects the relation of transmitter and receiver defined by $\mathbf{Z}_{RT}$. One representative of the physical channel $\mathbf{H}$ is the 'path-based' channel models used in [16]. A similar physical channel model is adopted in [27]. When the number of paths of the channel model in [16] increases to infinity, i.e., both the transmitter and receiver are in rich scattering environment, the correlation of the individual channels can be expressed statistically. Besides the MC effect, the correlation of each compact link end can come from the propagation channel characteristics and the array configuration.If the transmitter does not affect the spatial properties of the received signal at all, $\mathbf{H}$ becomes a Kronecker model with the following covariance structure [30]

$$E\left\{(\mathbf{H})_{ik}(\mathbf{H})_{jl}^*\right\} = c\,(\mathbf{\Psi}_T)_{kl}\,(\mathbf{\Psi}_R)_{ij} \tag{10}$$

where c is the average power gain of each channel branch (identical gain is assumed), $\mathbf{\Psi}_T$ and $\mathbf{\Psi}_R$ are $N \times N$ transmit and receive covariance matrices, respectively [4] with $\left|(\mathbf{\Psi}_T)_{ij}\right|$, $\left|(\mathbf{\Psi}_R)_{ij}\right| \leq 1$ and $(\mathbf{\Psi}_T)_{ii}$, $(\mathbf{\Psi}_R)_{ii} = 1$, $i, j = 1, 2, ..., N$. The Kronecker model has been used in [11], [12] to express $\mathbf{Z}_{RT}$ statistically. In this paper, the Kronecker channel model is assumed.

If $c = 1$ is assumed in (10), the MIMO channel $\mathbf{H}$ should be normalized to the average channel gain of a SISO system. Consider a SISO system with both antennas self-conjugated matched, i.e. $z_L = z_{11}^*$, where z_L and z_{11} is the load and self impedance of the antenna, respectively. Utilizing (6) and (8) we obtain the normalization factor of the MIMO channel $\mathbf{H}$ is $\frac{1}{4r_{11}^2}E\{hh^*\}$, where

h is the SISO channel and $r_{11} = \mathrm{Re}\{z_{11}\}$. Thus, the general MIMO system channel transfer matrix of Fig. 1 represented in Z-parameters is

$$\hat{\mathbf{H}}_{mc} = 2r_{11}\mathbf{R}_L^{1/2}\mathbf{Z}_{L+R}^{-1}\mathbf{\Psi}_R^{1/2}\mathbf{H}_{i.i.d.}\mathbf{\Psi}_T^{1/2}\mathbf{R}_T^{-1/2}. \tag{11}$$

We assume the major source of noise is the receiver front end [16]. The MIMO capacity with the channel matrix given by (13) is

$$C_{mc} = \log_2 \det\left(\mathbf{I}_N + \frac{\rho_r}{N}\hat{\mathbf{H}}_{mc}\hat{\mathbf{H}}_{mc}^H\right) \tag{12}$$

where ρ_r is the reference SNR.

In the following sections we focus on the compact receive end of the MIMO system with SPM. We further assume that the transmit antennas are sufficiently separated, rich scattering, i.e. $\mathbf{\Psi}_T = \mathbf{I}_N$, and self-conjugate matched. For a 2×2 MIMO system (11) can be simplified as

$$\hat{\mathbf{H}}_{mc} = 2\sqrt{r_{11}r_L}\mathbf{Z}_{L+R}^{-1}\mathbf{\Psi}_R^{1/2}\mathbf{H}_{i.i.d.} \tag{13}$$

where $r_L = \mathrm{Re}\{z_L\}$. Equation (13) is identical to the 2×2 channel matrix used in [10], [20], which is a special case of the MIMO channel matrix in (11).

III. Derivation of Optimal Single-Port Matching Impedance

The optimal single-port matching impedance $z_{opt} = r_{opt} + jx_{opt}$ which maximizes the mean capacity $E\{C_{mc}\}$ of a 2×2 MIMO system is derived in this section. As a random channel matrix is in (12), Jensen's inequality and the concavity of $\log_2\det$ [31] are used to achieve the upper bound C_{up} [32] for any fixed antenna spacing d as

$$E\left\{C_{mc}\right\} \leq C_{up} = \log_2 \det\left(\mathbf{I}_N + \frac{4\rho_r r_{11} r_L}{N}\mathbf{Z}_{L+R}^{-H}\mathbf{Z}_{L+R}^{-1}\mathbf{\Psi}_R\right). \tag{14}$$

We define the antenna self-impedance $z_{11} = r_{11} + jx_{11}$, mutual-impedance $z_{12} = r_{12} + jx_{12}$, load impedance $z_L = r_L + jx_L$, where the resistance components r_{11}, r_{12}, $r_L \in \mathbb{R}^+$ and the reactance components x_{11}, x_{12}, $x_L \in \mathbb{R}$. For identical antenna elements, we have $(\mathbf{Z}_{RR})_{ij} = (\mathbf{Z}_{RR})_{ji}$ based on the reciprocity theorem[1] [33]. Given a particular d and ρ_r, (14) becomes a

[1]We note that the reciprocity theorem is independent of the assumptions about the transmission environment. The FF pattern of the array does change in different scenarios, i.e. the variations of the mean AOA and angular spread (AS). This effect is reflected in the correlation matrix $\mathbf{\Psi}_R$.

function of variables (r_L, x_L). Then the matrix product $\mathbf{Z}_{L+R}^{-H}\mathbf{Z}_{L+R}^{-1}$ in (14) can be simplified as

$$\begin{aligned}\mathbf{Z}_{L+R}^{-H}\mathbf{Z}_{L+R}^{-1} &= \left(\left[\mathbf{Z}_{RR}+\mathbf{Z}_L\right]\left[\mathbf{Z}_{RR}+\mathbf{Z}_L\right]^H\right)^{-1} = \left(\left[\mathbf{Z}_{RR}+z_L\mathbf{I}_N\right]\left[\mathbf{Z}_{RR}^H+z_L^*\mathbf{I}_N\right]\right)^{-1} \\ &= \Big(\underbrace{|z_L|^2\mathbf{I}_N}_{\mathbf{Z}_1}+\underbrace{z_L\mathbf{Z}_{RR}^H+z_L^*\mathbf{Z}_{RR}}_{\mathbf{Z}_2}+\underbrace{\mathbf{Z}_{RR}\mathbf{Z}_{RR}^H}_{\mathbf{Z}_3}\Big)^{-1}. \end{aligned} \tag{15}$$

Expanding (15) we have

$$\begin{aligned}\mathbf{Z}_1 &= \begin{bmatrix} r_L^2+x_L^2 & 0 \\ 0 & r_L^2+x_L^2 \end{bmatrix} \\ \mathbf{Z}_2 &= 2\left(r_L\cdot\begin{bmatrix} r_{11} & r_{12} \\ r_{12} & r_{11}\end{bmatrix}+x_L\cdot\begin{bmatrix} x_{11} & x_{12} \\ x_{12} & x_{11}\end{bmatrix}\right) \\ \mathbf{Z}_3 &= \begin{bmatrix} r_{11}^2+x_{11}^2+r_{12}^2+x_{12}^2 & 2(r_{11}r_{12}+x_{11}x_{12}) \\ 2(r_{11}r_{12}+x_{11}x_{12}) & r_{11}^2+x_{11}^2+r_{12}^2+x_{12}^2\end{bmatrix}\end{aligned} \tag{16}$$

Lemma 1: For any real symmetric Toeplitz matrix $\mathbf{A}$, the singular value decomposition (SVD) of $\mathbf{A}$ can be written as $\mathbf{A} = \mathbf{U}\mathbf{D}\mathbf{U}^{\mathbf{T}} = \mathbf{U}\mathbf{D}\mathbf{U}$, where

$$\mathbf{A} = \begin{bmatrix} a_1 & a_2 \\ a_2 & a_1\end{bmatrix}, \mathbf{U} = \frac{1}{\sqrt{2}}\begin{bmatrix} 1 & 1 \\ 1 & -1\end{bmatrix}, \mathbf{D} = \begin{bmatrix} a_1+a_2 & 0 \\ 0 & a_1-a_2\end{bmatrix}.$$

Proof: $\mathbf{A}$ is a 2×2 circulant matrix. Following [34], the eigenvalue solution of $\mathbf{A}$ is $\lambda_k = a_1 + a_2 r_k$, $k = 1, 2$, and r_k is the kth complex root of $r^2 = 1$. The corresponding eigenvector $u_k = 2^{-1/2}[1, r_k]^T$. Then $\mathbf{U} = [u1, u2]$, and $\mathbf{U}$ is unitary. ■

Utilizing Lemma 1, the singular value decomposition (SVD) of (15) is given

$$\begin{aligned}\mathbf{Z}_{L+R}^{-H}\mathbf{Z}_{L+R}^{-1} =& \Bigg(\mathbf{U}\Bigg(\begin{bmatrix} r_L^2+x_L^2 & 0 \\ 0 & r_L^2+x_L^2\end{bmatrix}+2r_L\cdot\begin{bmatrix} \mathfrak{R}_1 & 0 \\ 0 & \mathfrak{R}_2\end{bmatrix} \\ &+2x_L\cdot\begin{bmatrix} \mathfrak{X}_1 & 0 \\ 0 & \mathfrak{X}_2\end{bmatrix}+\begin{bmatrix} \mathfrak{R}_1^2+\mathfrak{X}_1^2 & 0 \\ 0 & \mathfrak{R}_2^2+\mathfrak{X}_2^2\end{bmatrix}\Bigg)\mathbf{U}\Bigg)^{-1} \\ =& \mathbf{U}\begin{bmatrix} (r_L+\mathfrak{R}_1)^2+(x_L+\mathfrak{X}_1)^2 & 0 \\ 0 & (r_L+\mathfrak{R}_2)^2+(x_L+\mathfrak{X}_2)^2\end{bmatrix}^{-1}\mathbf{U} = \mathbf{U}\mathbf{\Lambda}^{-1}\mathbf{U}\end{aligned} \tag{17}$$

where $\mathfrak{R}_1 = r_{11}+r_{12}$, $\mathfrak{X}_1 = x_{11}+x_{12}$, $\mathfrak{R}_2 = r_{11}-r_{12}$, $\mathfrak{X}_2 = x_{11}-x_{12}$. Using the property $\det(\mathbf{I}+\mathbf{A}\mathbf{B}) = \det(\mathbf{I}+\mathbf{B}\mathbf{A})$ [3], (14) can be rewritten as

$$C_{up} = \log_2\det(\mathbf{I}_N + \kappa r_L\cdot\mathbf{U}\mathbf{\Lambda}^{-1}\mathbf{U}\mathbf{\Psi}) = \log_2\det(\mathbf{I}_N+\kappa\mathbf{U}\mathbf{\Psi}\mathbf{U}r_L\mathbf{\Lambda}^{-1}) = \log_2\det(\mathbf{Y}) \tag{18}$$

where $\kappa = \rho_r \cdot 4r_{11}/N$. According to the monotonically increasing characteristic of $\log_2(\cdot)$, the maximum point of $\det(\cdot)$ is the maximum point of $\log_2\det(\cdot)$. To derive the maximum point (r_{opt}, x_{opt}) of $\det(\mathbf{Y})$, we evaluate the following derivatives

$$\frac{\partial \det(\mathbf{Y})}{\partial r_L} = \kappa \cdot \frac{(\mathfrak{R}_1^2 - r_L^2 + (x_L + \mathfrak{X}_1)^2) \cdot \Sigma_2 + (\mathfrak{R}_2^2 - r_L^2 + (x_L + \mathfrak{X}_2)^2) \cdot \Sigma_1}{\left(\left((r_L + \mathfrak{R}_1)^2 + (x_L + \mathfrak{X}_1)^2\right)\left((r_L + \mathfrak{R}_2)^2 + (x_L + \mathfrak{X}_2)^2\right)\right)^2} \tag{19a}$$

$$\frac{\partial \det(\mathbf{Y})}{\partial x_L} = -2\kappa r_L \cdot \frac{(x_L + \mathfrak{X}_1) \cdot \Sigma_2 + (x_L + \mathfrak{X}_2) \cdot \Sigma_1}{\left(\left((r_L + \mathfrak{R}_1)^2 + (x_L + \mathfrak{X}_1)^2\right)\left((r_L + \mathfrak{R}_2)^2 + (x_L + \mathfrak{X}_2)^2\right)\right)^2} \tag{19b}$$

where

$$\begin{aligned}
\Sigma_1 &= \left((r_L + \mathfrak{R}_1)^2 + (x_L + \mathfrak{X}_1)^2\right) \cdot \left((1 - \mathrm{Re}\{\alpha\})\left((r_L + \mathfrak{R}_1)^2 + (x_L + \mathfrak{X}_1)^2\right) + (1 - |\alpha|^2)\kappa r_L\right), \\
\Sigma_2 &= \left((r_L + \mathfrak{R}_2)^2 + (x_L + \mathfrak{X}_2)^2\right) \cdot \left((1 + \mathrm{Re}\{\alpha\})\left((r_L + \mathfrak{R}_2)^2 + (x_L + \mathfrak{X}_2)^2\right) + (1 - |\alpha|^2)\kappa r_L\right),
\end{aligned} \tag{20}$$

and $\alpha = (\mathbf{\Psi}_R)_{12} = (\mathbf{\Psi}_R)_{21}$. In (20) it can be shown that $\forall \Sigma_{1,2} > 0$. As the maximum point (r_{opt}, x_{opt}) makes (19) equal to zero, then from (19b) we can deduce

$$x_{opt} \in [\min(-\mathfrak{X}_1, -\mathfrak{X}_2), \max(-\mathfrak{X}_1, -\mathfrak{X}_2)]. \tag{21}$$

Substituting (21) into (19a) we have

$$r_{opt} \in [\min(\mathfrak{R}_1, \mathfrak{R}_2), \max(\sqrt{\mathfrak{R}_1^2 + (\mathfrak{X}_1 - \mathfrak{X}_2)^2}, \sqrt{\mathfrak{R}_2^2 + (\mathfrak{X}_1 - \mathfrak{X}_2)^2})]. \tag{22}$$

Solving (19a) and (19b) the simple relation between r_L and x_L can be obtained

$$r_L^2 + (x_L + \sigma)^2 = \Gamma. \tag{23}$$

Geometrically, (r_{opt}, x_{opt}) is a point on the circumference of a circle with the center at $(0, -\sigma)$ and radius $\sqrt{\Gamma}$, where $\sigma = x_{11} + \frac{r_{11}r_{12}}{x_{12}}, \Gamma = r_{11}^2 + r_{12}^2 + x_{12}^2 + \frac{r_{11}^2 r_{12}^2}{x_{12}^2}$. Combined with (21) and (22), (r_{opt}, x_{opt}) can be restricted to be located in an arc of the circle.

Substituting (23) into (19b), we can deduce a polynomial in x_L

$$\sum_{m=0}^{8} p_m x_L^m = \sum_{m=0}^{8} f_m(\mathfrak{R}_1, \mathfrak{X}_1, \mathfrak{R}_2, \mathfrak{X}_2, \sigma, \Gamma, \kappa) x_L^m = \sum_{m=0}^{8} g_m(r_{11}, x_{11}, r_{12}, x_{12}, \rho_r) x_L^m = 0 \tag{24}$$

where the coefficients p_m are determined by the high order polynomials $f_m(\mathfrak{R}_1, \mathfrak{X}_1, \mathfrak{R}_2, \mathfrak{X}_2, \sigma, \Gamma, \kappa)$ = $g_m(r_{11}, x_{11}, r_{12}, x_{12}, \rho_r)$. We summarize the derivation of z_{opt} in following steps:

Step 1. Solving (24) to find all the roots of x_L;

Step 2. Filtering the results of **Step 1** by (21);

Step 3. Substituting the results of **Step 2** into (23) to get the corresponding roots of r_L;

Step 4. Filtering the results of **Step 3** by (22).

In high SNR regime, (18) can be simplified as

$$C_{up} = \log_2 \det(\kappa \mathbf{U}\mathbf{\Psi}\mathbf{U} r_L \mathbf{\Lambda^{-1}}) = \log_2 \det(\mathbf{Y}) \tag{25}$$

where $\det(\mathbf{Y}) = \frac{(\mathbf{1}-\alpha^{\mathbf{2}})}{\det(\mathbf{\Lambda})}$. The derivatives in (19) are modified by simplifying (20) as

$$\Sigma_i = (r_L + \mathfrak{R}_i)^2 + (x_L + \mathfrak{X}_i)^2, \qquad i = 1, 2. \tag{26}$$

Solving the equations we derive the closed-form of $z_{opt} = r_{opt} + j x_{opt}$, where

$$r_{opt} = \sqrt{\mathfrak{R}_1\mathfrak{R}_2\left(1 + \frac{(\mathfrak{X}_1 - \mathfrak{X}_2)^2}{(\mathfrak{R}_1 + \mathfrak{R}_2)^2}\right)} = \sqrt{r_{11}^2 - r_{12}^2 + x_{12}^2 - \frac{r_{12}^2 x_{12}^2}{r_{11}^2}} \tag{27a}$$

$$x_{opt} = -\frac{\mathfrak{R}_1\mathfrak{X}_2 + \mathfrak{R}_2\mathfrak{X}_1}{\mathfrak{R}_1 + \mathfrak{R}_2} = \frac{r_{12}x_{12}}{r_{11}} - x_{11} \tag{27b}$$

This solution of z_{opt} is exactly the input impedance (z_{in}) match in [22]. It is shown that in a high SNR scenario, z_{opt} is an exact solution only related to the array impedances and independent from the open-circuit (OC) correlation α which provides the possibility of practical implementation. The finding of $z_{in} = z_{opt}$ in high SNR case is under prediction because from circuit theory considerations it includes the MC effect into the matching network [35], which realizes the maximum power transfer between the corresponding source and receiver within the SPM range. Moreover, it gives low correlation for any antenna separation [22].

IV. Simulation and Analysis

A 2×2 MIMO system using ideal half-wavelength ($\lambda/2$) dipoles [2] equipped at both ends is deployed to demonstrate the analytical results in Section III. The optimal single-port impedances z_{opt} generated by Monte Carlo simulations of the same MIMO system model for both ergodic capacity C_{mc} are compared to the results simulated using the upper bound C_{up} as well as the numerical results of Section III. The superiority of using z_{opt} to other matching networks in the MIMO system is also discussed.

[2]Ideal half-wavelength dipoles are adopted because their self and mutual impedances are easily computed numerically. The impedance matrices of other kinds of antennas obtained either analytically or experimentally can be applied as well.

The self and mutual impedances z_{11}, z_{12} of the ideal $\lambda/2$ dipoles are calculated numerically using the modified EMF method [3] [5]. Choosing a reference SNR ρ_r and substituting the values of z_{11}, z_{12} into polynomials g_m in (24), we can get multiple solutions of x_L for each antenna spacing d. After the values of x_L are filtered by the range (21) (Fig. 2(a)), the corresponding results of r_L can be computed by (23). Fig. 3 depicts the arc of possible locations for (r_{opt}, x_{opt}) utilizing (23) at $d = 0.05\lambda$. The abscissa of Fig. 3 is determined by r_{Lmin} = min($\mathfrak{R}_2$) and r_{Lmax} = max($\sqrt{\mathfrak{R}_1^2 + (\mathfrak{X}_1 - \mathfrak{X}_2)^2}$) according to Fig. 2(b). In Fig. 3 it is obvious that $x_{Lmax} = -\mathfrak{X}_2 = -17.9\ \Omega$, therefor x_L can not reach zero as in Fig. 2(a), and the lower bound of x_L in Fig. 3 is modified to $x_{Lmin} = \min(-\mathfrak{X}_1)|_{-\mathfrak{X}_2 \leq -17.9}$. Finally, the desirable solution (r_{opt}, x_{opt}) can be obtained using (22) (Fig. 2(b)). When d is fixed, the unique solution is a point on the arc, and the position of (r_{opt}, x_{opt}) depends on the value of ρ_r.

Monte Carlo simulations for the ergodic capacity C_{mc} in (12) and the upper bound C_{up} in (14) are used to verify the derivation in Section III. If uniform distributed power azimuth spectrum (PAS) is assumed at the receiver, the correlation $\alpha = J_0(2\pi d/\lambda)$ [37], where $J_0(\cdot)$ is the zeroth order Bessel function of the first kind. As the numerical z_{opt} is the maximum point of C_{up} rather than C_{mc}, the simulation results of z_{opt} for both cases are plotted in Fig. 4. The range of $\{z_L = r_L + jx_L : r_L \in [0, 150]\Omega, x_L \in [-100, 50]\Omega\}$ is chosen to get the z_{opt} of each C_{up}. The C_{mc} is simulated over 10000 random channel realizations for every z_L point at each d, thereby the range of z_L is shrunk to a few ohms around the z_{opt} of C_{up} to save computing time. In Fig. 4 it is apparent that the numerically derived z_{opt} agrees well with the corresponding simulation results of C_{up} and C_{mc}. Moreover, the z_{opt} approaches the input impedance z_{in} as ρ_r increases, which is perfectly consistent with the derivation in Section III. Another observation is that the x_{opt} is hardly affected by ρ_r and the impact of ρ_r on the r_{opt} diminishes when $d > 0.2\lambda$.

Because the numerical values of z_{opt} match very well to the simulation results of both C_{up} and C_{mc} cases, the precise data of z_{opt} is presented in Table I. For the resistive component r_{opt}, the numerical and simulation results differ from each other for $d \leq 0.2\lambda$ with a maximum error of less than 1Ω. The errors decrease while ρ_r increases. When $d \geq 0.3\lambda$, the numerical and simulation r_{opt} of C_{up} are equal with no error. Meanwhile, the numerical r_{opt} experiences an

[3]Infinite thin dipoles are assumed for the EMF calculations as the dipole diameter is usually far less than its length. Similar self and mutual impedance results of practical dipole cases can be found in [16], [36]. As our focus is on the relative ratio of the self and mutual impedances, ideal dipoles are selected for simplicity.

maximum error of 0.4Ω compared to the simulation r_{opt} of C_{mc} for any value of ρ_r. For the reactive component x_{opt}, the numerical x_{opt} is equal to the simulation x_{opt} of C_{up} with no error for all values of ρ_r. The x_{opt} of C_{mc} has an maximum error of 0.4Ω compared to the other two cases due to the limited number of realizations of the Monte Carlo simulation. Both Fig. 4 and Table I confirm that the analytical study in Section III can predict z_{opt} of the C_{mc} correctly, as well as yield z_{opt} of the C_{up} accurately and more efficiently than the Monte Carlo C_{mc}. Values of the z_{in} are in Table I agree well with the corresponding values of z_{opt} at $\rho = 20$dB, which proves the analytical finding of the high SNR case in Section III.

To illustrate the MIMO system benefit from the z_{opt} match, the C_{mc} and C_{up} with the characteristic impedance match of both no coupling (z_{0nc}) and MC (z_0) cases, ${z_{11}}^*$, z_{in} and z_{opt} matches are depicted with different values of ρ_r in Fig. 5. Fig. 5 illustrates using a matching network to optimize C_{up} also optimizes C_{mc}. When $\rho_r = 5$dB (Fig. 5(a)), the performance of the receivers without MC is always better than that with MC. However, for $\rho_r = 20$dB case (Fig. 5(b)), the compact receiver with any matching network outperforms that without MC at $d < 0.2\lambda$. Meanwhile, the z_{opt} match surpasses other matching schemes when $d < 0.25\lambda$ and overlaps with the z_{11}^* match and z_{in} match at $d \geq 0.25\lambda$ in both low and high SNR scenarios. The performance of the z_{opt} match outperforms that of the z_{in} match only at $d < 0.1\lambda$ in Fig. 5(a). With increasing SNR in Fig. 5(b), the performance of z_{opt} and z_{in} overlap with each other at all antenna spacings, which again verifies the analysis in Section III. It is obvious that r_{opt} is the dominant factor which determines the value of C_{up} in Fig. 5 because C_{up} follows the monotonically increasing property of r_{opt} in Fig. 4 with all spacings. This can be explained because r_{opt} is the part of z_{opt} receiving the power which contains the mutual information.

V. Experimental Validation

We further present measured antenna impedances z_{11},z_{12} and OC correlation results α to validate the analytical results in Section III. The experimental setup of a compact receive array is shown in Fig. 6. Two quarter-wavelength monopoles with $d = 0.05\lambda, 0.1\lambda, 0.15\lambda$ and a center frequency of 900MHz are mounted on a 330mm $\times$ 250mm ground plane. Both brass antennas of identical dimensions (diameter of 2mm) are soldered onto 50Ω matching network boards with the output ports of SMA connectors soldered onto the opposite end. The z_{11} of a single monopole and the z_{11}, z_{12} of the monopole array are measured by a network analyzer. To calculate α addressed

in Section II, the two-dimensional (2D) FF patterns of the monopole array with OC terminations are measured in an anechoic chamber at Perlos AB, Sweden[4]. An identical receive system model is simulated in SEMCAD [38] using finite-difference time-domain (FDTD) analysis.

There are no analytical equations for the z_{11} and z_{12} of monopoles on a finite ground plane. Fig. 7 displays the results of z_{11} and z_{12} of the monopole array from both simulation and measurement. The simulation results are derived from the open and short-circuit impedances [6], while the experimental results are transferred from the S-parameter data observed at the network analyzer. Because in practice the monopoles cannot be exactly identical, the average values of the measured z_{11} and z_{12} are shown in Fig. 7 as well. The close match of the measured results of both monopoles ensures the validity of further experiment. The simulation and the average of the measured results also show great consistency in Fig. 7. Meanwhile, with increasing d, the difference between the simulation and the average of the measured results decreases. In the following part, we focus on the antenna spacing of $d = 0.05\lambda$, where the self and mutual impedances of the monopoles are $z_{11} = 47.5 + j10.9\Omega$, $z_{12} = 46.77 - j0.57\Omega$ in simulation, and $z_{11} = 46.72 + j9.39\Omega$, $z_{12} = 45.31 - j2.57\Omega$ on average in measurement. The corresponding values of α are 0.9796 in SEMCAD and 0.959 in measurement calculated from the FF patterns.

Table II lists the ergodic capacity C_{mc} generated using antenna parameters from simulation and measurement with different matching networks. The loads z_A and z_B are selected from the area of optimum impedances for received power maximization, while z_C and z_D are picked from the approximately zero correlation circle [25]. The z_0 of 50Ω is also chosen. For the z_{11}^*, z_{in} and the z_{opt} matches, there are two sets of impedances shown based on the corresponding z_{11}, z_{12} and α obtained in simulation and measurement, respectively. The notation z_{opt}^n in Table II represents the numerical z_{opt} results of Section III. We note that the same number of channel realizations and 20dB reference SNR ρ_r are used in generating C_{mc}. The values of z_{11}^* of a single monopole listed in Table II are used for power normalization of the corresponding cases, because the z_{11} of an isolated antenna differs from that in the array [16], [36].

Generally, the C_{mc} generated using the measured resutls are about 0.5 bits/s/Hz higher than the corresponding simulation results of each load point. Apparently, none of the impedances either

[4]Though the channel in the chamber is LOS, the FF patterns are measured over 2π radians. This is consistent with a MIMO NLOS channel with uniformly distributed PAS and full AS. Thus the measured correlation can be used in this paper.

maximizing the received power or achieving zero output correlation maximize the capacity, which confirms the finding in [10], [20]. Among these impedances, z_D offers the best performance as it is chosen to be the load with the highest received power along the zero correlation circle, and also because it is close to z_{opt}. Also, the commonly used z_0 and z_{11}^* give inferior performance to the corresponding z_{in} match of 0.5 bits/s/Hz. Furthermore, the numerical z_{opt} agree well with the corresponding simulation results, which again confirms the analytical study in Section III. The error between the corresponding numerical and simulation results of z_{opt} is within 1Ω, which is caused by the deviation between z_{11} of the single antenna and z_{11} used in the array. When a high SNR (ρ_r = 20dB) is assumed, both numerical and simulation results of z_{opt} agree well with the corresponding z_{in}, especially in the measurement. As shown in Table I, the errors between the numerical and simulation results of z_{opt} as well as z_{in} decrease when d increases, we are confident of the validity of our derivation with larger antenna separations.

VI. Conclusion

This paper derives the optimal single-port matching impedance (z_{opt}) for capacity maximization of a 2×2 MIMO system with coupled receiver using Z-parameters. Closed-form solutions of z_{opt} for the high SNR scenario is deduced and confirmed to be the input matching impedance of the receive antenna. We have shown that the analytical and simulation results agree well with each other through the example of ideal dipoles. By introducing z_{opt} into a MIMO system with two coupled dipoles, the ergodic capacity has an advantage of around 1 bit/s/Hz for antenna spacings less than 0.25λ compared to the commonly used characteristic match when the SNR is 20dB. An experimental setup of a monopole array is also introduced to verify the analytical study. It is shown that a capacity benefit of 0.5 bits/s/Hz can be achieved over the commonly used self-conjugate match for an antenna element spacing 0.05λ at 20dB SNR.

We conclude that the MIMO system performance can be significantly improved by integrating z_{opt} into compact arrays at close antenna separations. More research can done for compact receivers with larger sizes and different configurations to explore the existence of z_{opt}. The MIMO channel matrix using Z-parameters and the method of finding z_{opt} presented in this paper offers a good chance to solve these problems. In later work, the same methodology used in this paper may be applied to find optimal noise-figure loading for more realistic amplifiers [27]. A measurement campaign involving direct MIMO channel measurements (including the

effect of the matching network) and measured capacity evaluation is also an interesting aspect for future work.

ACKNOWLEDGMENT

The authors would like to thank Prof. Andreas Molisch of the Department of Electrical and Information Technology, Lund University for reviewing the paper and giving valuable feedback. Many thanks to Mr. Jie Ding of the Institute for Digital Communications, the University of Edinburgh for useful discussions. Also we thank Dr. Anders Sunesson of Perlos AB, Lund, Sweden for providing the facility and expertise to measure the antenna FF patterns, and Mr. Lars Hedenstjärna of the Department of Electrical and Information Technology, Lund University for technical advice and construction of the experimental hardware.

This work is supported by Scottish Funding Council for the Joint Research Institute with the Heriot-Watt University (a part of the Edinburgh Research Partnership), VINNOVA (grant no. 2007-01377), and NEWCOM (Network of Excellence in Communications).

REFERENCES

[1] J. Winters, "On the capacity of radio communication systems with diversity in a rayleigh fading environment," *IEEE J. Select. Areas Commun.*, vol. 5, pp. 871–878, 1987.

[2] G. J. Foschini and M. J. Gans, "On limits of wireless communications in a fading environment when using multiple antennas," *Wireless Personal Communications*, vol. 6, pp. 311–335, Mar. 1998.

[3] I. E. Telatar, "Capacity of multi-antenna gaussian channels," *European Trans. Telecommun.*, vol. 10, pp. 585–595, 1999.

[4] A. Paulraj, R. Nabar, and D. Gore, *Introduction to space-time wireless communications*, 1st ed. Cambridge, UK: Cambridge University Press, 2003.

[5] C. A. Balanis, *Antenna theory*, 2nd ed., S. Elliot, Ed. USA: John Wiley & Sons, Inc, 1997.

[6] W. L. Stutzman and G. A. Thiele, *Antenna theory and design*, 2nd ed. New York, USA: John Wiley & Sons, Inc., 1998.

[7] R. G. Vaughan and J. B. Andersen, "Antenna diversity in mobile communications," *IEEE Trans. Veh. Technol.*, vol. VT-36, no. 4, pp. 149–172, Nov. 1987.

[8] T. Svantesson and A. Ranheim, "Mutual coupling effects on the capacity of multielement antenna systems," in *Proceedings of IEEE International Conference on Acoustics, Speech and Signal Processing (ICASSP'01)*, vol. 4, Salt Lake City, UT, May 7-11, 2001, pp. 2485–2488.

[9] J. W. Wallace and M. A. Jensen, "Termination-dependent diversity performance of coupled antennas: Network theory analysis," *IEEE Trans. Antennas Propagat.*, vol. 52, no. 1, pp. 98–105, January 2004.

[10] B. K. Lau, J. B. Andersen, G. Kristensson, and A. F. Molisch, "Antenna matching for capacity maximization in compact MIMO systems," in *Proceedings of 3rd International Symposium on Wireless Communications Systems (ISWCS)*, Valencia, Spain, Sept. 6-8, 2006, pp. 253–257.

[11] R. Janaswamy, "Effect of element mutual coupling on the capacity of fixed length linear arrays," *IEEE Antennas Wireless Propagat. Lett.*, vol. 1, pp. 157–160, 2002.

[12] N. Chiurtu, B. Rimoldi, E. Telatar, and V. Pauli, "Impact of correlation and coupling on the capacity of MIMO systems," in *Proceedings of 3rd IEEE International Symposium on Signal Processing and Information Technology (ISSPIT'03)*, Darmstadt, Germany, Dec. 14-17, 2003, pp. 154–157.

[13] B. Clerckx, D. Vanhoenacker-Janvier, C. Oestges, and L. Vandendorpe, "Mutual coupling effects on the channel capacity and the space-time processing of MIMO communication systems," in *Proceedings of IEEE International Conference on Communications (ICC'03)*, vol. 4, Seattle, WA, May 11-15, 2003, pp. 2638–2642.

[14] V. Jungnickel, V. Pohl, and C. V. Helmolt, "Capacity of MIMO systems with closely spaced antennas," *IEEE Commun. Lett.*, vol. 7, no. 8, pp. 361–363, August 2003.
[15] P. N. Fletcher, M. Dean, and A. R. Nix, "Mutual coupling in multi-element array antennas and its influence on MIMO channel capacity," *IEE Electronics Letters*, vol. 39, no. 4, pp. 342–344, February 2003.
[16] J. W. Wallace and M. A. Jensen, "Mutual coupling in MIMO wireless systems: a rigorous network theory analysis," *IEEE Trans. Wireless Commun.*, vol. 3, no. 4, pp. 1317–1325, July 2004.
[17] C. Waldschmidt, S. Schulteis, and W. Wiesbeck, "Complete RF system model for analysis of compact MIMO arrays," *IEEE Trans. Veh. Technol.*, vol. 53, no. 3, pp. 579–586, May 2004.
[18] E. A. Mehmet Kemal Özdemir and H. Arslan, "Dynamics of spatail correlation and implications on MIMO systems," *IEEE Commun. Mag.*, pp. 514–519, 2004.
[19] S. Wei, D. Goeckel, and R. Janaswamy, "On the asymptotic capacity of MIMO systems with antenna arrays of fixed length," *IEEE Trans. Wireless Commun.*, vol. 4, no. 4, pp. 1608–1621, 2005.
[20] B. K. Lau and J. B. Andersen, "On closely coupled dipoles with load matching in a random field," in *Proceedings of IEEE 17th International Symposium on Personal, Indoor and Mobile Radio Communications (PIMRC'06)*, Helsinki, Finland, Sept. 11-14, 2006.
[21] B. K. Lau, S. M. S. Ow, G. Kristensson, and A. F. Molisch, "Capacity analysis for compact MIMO systems," in *Proceedings of IEEE 61st Vehicular Technology Conference (VTC'05-Spring)*, vol. 1, Stockholm, Sweden, May 30-June 1, 2005, pp. 165–170.
[22] B. K. Lau, J. B. Andersen, G. Kristensson, and A. F. Molisch, "Impact of matching network on bandwidth of compact antenna arrays," *IEEE Trans. Antennas Propagat.*, vol. 54, no. 11, pp. 3225 – 3238, Nov. 2006.
[23] W. C.-Y. Lee, "Effect of mutual coupling on a mobile-radio maximum ratio diversity combiner with a large number of branches," *IEEE Trans. Commun.*, pp. 1188–1193, Dec. 1972.
[24] J. B. Andersen and B. K. Lau, "On closely coupled dipoles in a random field," *IEEE Antennas Wireless Propagat. Lett.*, vol. 5, pp. 73–75, 2006.
[25] Y. Fei, B. K. Lau, A. Sunesson, A. J. Johansson, J. B. Andersen, and J. S. Thompson, "Experiments of closely coupled monopoles with load matching in a random field," in *Proceedings of 1st European Conference of Antenna and Propagation (EUCAP'06)*, Nice, France, Nov. 6-10, 2006.
[26] M. L. Morris and M. A. Jensen, "Improved network analysis of coupled antenna diversity performance," *IEEE Trans. Wireless Commun.*, vol. 4, no. 4, pp. 1928–1934, 2005.
[27] ——, "Network model for MIMO systems with coupled antennas and noisy amplifiers," *IEEE Trans. Antennas Propagat.*, vol. 53, no. 1, pp. 545–552, Jan. 2005.
[28] ——, "Impact of receive amplifier signal coupling on MIMO system performance," *IEEE Trans. Veh. Technol.*, vol. 54, no. 5, pp. 1678–1683, Sept. 2005.
[29] Y. Fan and J. S. Thompson, "MIMO configurations for relay channels: Theory and practice," *IEEE Trans. Wireless Commun.*, vol. 6, no. 5, pp. 1774–1786, Mar. 2007.
[30] C.-N. Chuah, D. N. C. Tse, J. M. Kahn, and R. A. Valenzuela, "Capacity scaling in MIMO wireless systems under correlated fading," *IEEE Trans. Inform. Theory*, vol. 48, no. 3, pp. 637–650, Mar. 2002.
[31] T. M. Cover and J. A. Thomas, *Elements of information theory*, 2nd ed. USA: Jonh Wiley & Sons, Inc., 2006.
[32] S. Loyka and G. Tsoulos, "Estimating MIMO system performance using the correlation matrix approach," *IEEE Commun. Lett.*, vol. 6, no. 1, pp. 19–21, January 2002.
[33] J. D. Kraus, *Antennas*, 2nd ed. New York: McGraw-Hill, 1988.
[34] R. M. Gray, *Toeplitz and Circulant Matrices: A review*. USA: Now Publishers, Feb. 2006.
[35] K. Rosengren, J. Carlsson, and P.-S. Kildal, "Maximizing the effective diverstiy gain of two parallel dipoles by optimizing the source impedances," *Microwave and Optical Technology Letters*, vol. 48, no. 3, pp. 532–535, March 2006.
[36] S. M. S. Ow, "Impact of mutual coupling on compact MIMO systems," Master's thesis, Lund University, Lund, Sweden, March 2005.
[37] J. Salz and J. H. Winters, "Effect of fading correlation on adaptive arrays in digital mobile radio," *IEEE Trans. Veh. Technol.*, vol. 43, no. 4, pp. 1049–1057, November 1994.
[38] *SEMCAD*. [Online]. Available: http://www.semcad.com

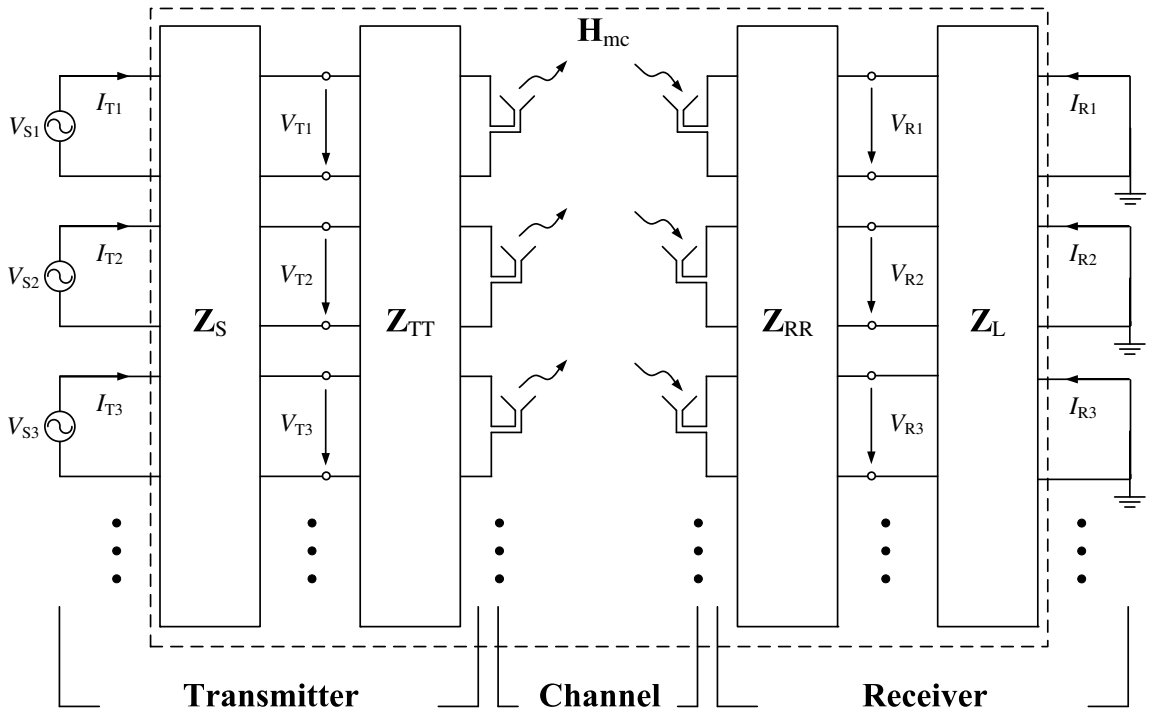

Fig. 1. Diagram of a MIMO system with antenna impedance matrices and matching networks at both link ends.

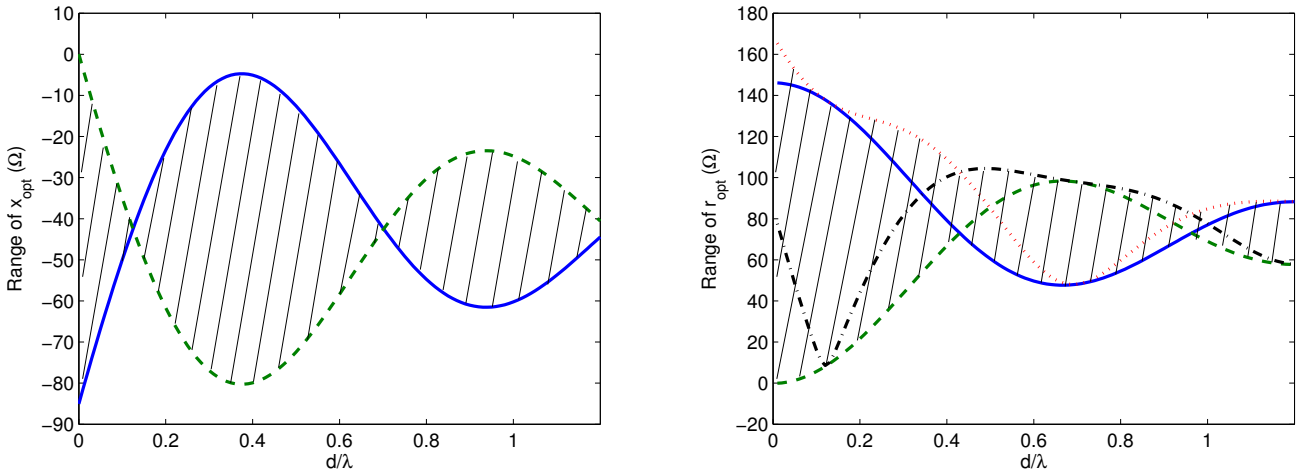

(a) (b)

Fig. 2. The possible range (shadow areas) of (r_{opt}, x_{opt}) of ideal $\lambda/2$ dipoles as a function of antenna spacing. In (a) x_{opt} varies between $-\mathfrak{X}_1$ (solid line) and $-\mathfrak{X}_2$ (dash line); in (b) r_{opt} moves among $\mathfrak{R}_1$ (solid line), $\mathfrak{R}_2$ (dash line), $\sqrt{\mathfrak{R}_1^2 + (\mathfrak{X}_1 - \mathfrak{X}_2)^2}$ (dot line) and $\sqrt{\mathfrak{R}_2^2 + (\mathfrak{X}_1 - \mathfrak{X}_2)^2}$ (dash-dot line).

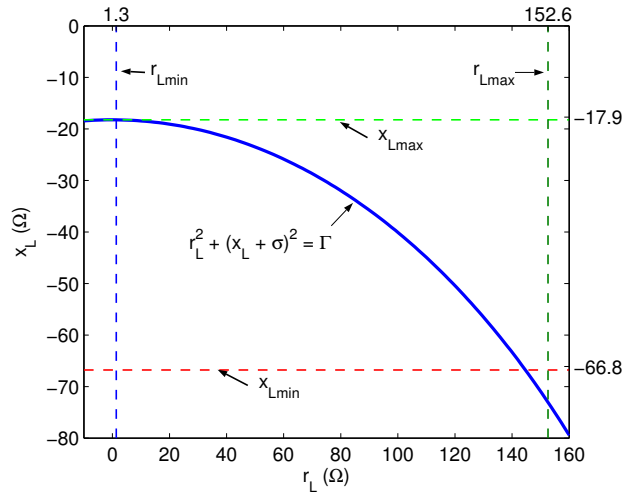

Fig. 3. Arc of the possible values of (r_{opt}, x_{opt}) for two compact ideal $\lambda/2$ dipoles of $d = 0.05\lambda$.

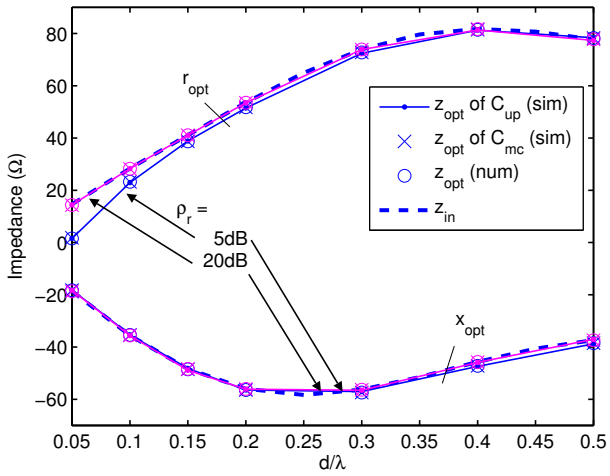

Fig. 4. The real and imaginary parts of numerical and simulation optimal single-port impedances compared to input impedance matching as a function of various antenna spacings with different ρ_r.

TABLE I

COMPARISON OF THE NUMERICAL AND SIMULATION RESISTANCE AND REACTANCE COMPONENTS OF THE OPTIMAL SINGLE-PORT IMPEDANCES WITH VARIOUS ANTENNA SPACINGS AND REFERENCE SNRS

d/λ	$r_{opt}(\Omega)$									$r_{in}(\Omega)$
	ρ_r = 5dB			ρ_r = 10dB			ρ_r = 20dB			
	num*	$\text{sim}^{\dagger}_{up}$	$\text{sim}^{\ddagger}_{m}$	num	sim_{up}	sim_{m}	num	sim_{up}	sim_{m}	
0.05	1.53	1.81	1.56	4.51	4.37	4.33	14.36	14.33	14.44	14.69
0.10	23.23	23.22	22.92	27.05	27.00	26.80	28.23	28.22	28.29	28.35
0.20	51.78	51.76	51.49	52.95	52.94	53.45	53.53	53.53	53.45	53.60
0.30	72.77	72.77	72.48	73.51	73.51	73.70	73.90	73.90	73.89	73.95
0.40	81.44	81.44	81.27	81.63	81.63	81.69	81.73	81.73	81.37	81.74
0.50	78.26	78.26	78.36	77.93	77.93	78.09	77.75	77.75	77.35	77.73
	$x_{opt}(\Omega)$									$x_{in}(\Omega)$
0.05	-18.23	-18.23	-18.16	-18.27	-18.27	-18.16	-18.66	-18.66	-18.26	-18.68
0.10	-35.35	-35.35	-35.30	-35.49	-35.49	-35.06	-35.54	-35.54	-35.62	-35.55
0.20	-56.46	-56.46	-56.44	-56.16	-56.17	-56.62	-56.02	-56.02	-56.12	-56.00
0.30	-57.44	-57.44	-57.05	-56.72	-56.73	-56.29	-56.35	-56.35	-56.57	-56.30
0.40	-47.21	-47.21	-47.39	-46.26	-46.26	-45.88	-45.75	-45.75	-45.88	-45.69
0.50	-38.54	-38.55	-38.77	-37.81	-37.81	-38.16	-37.41	-37.41	-37.07	-37.36

*numerical results †simulation results based on C_{up} ‡simulation results based on C_{mc}

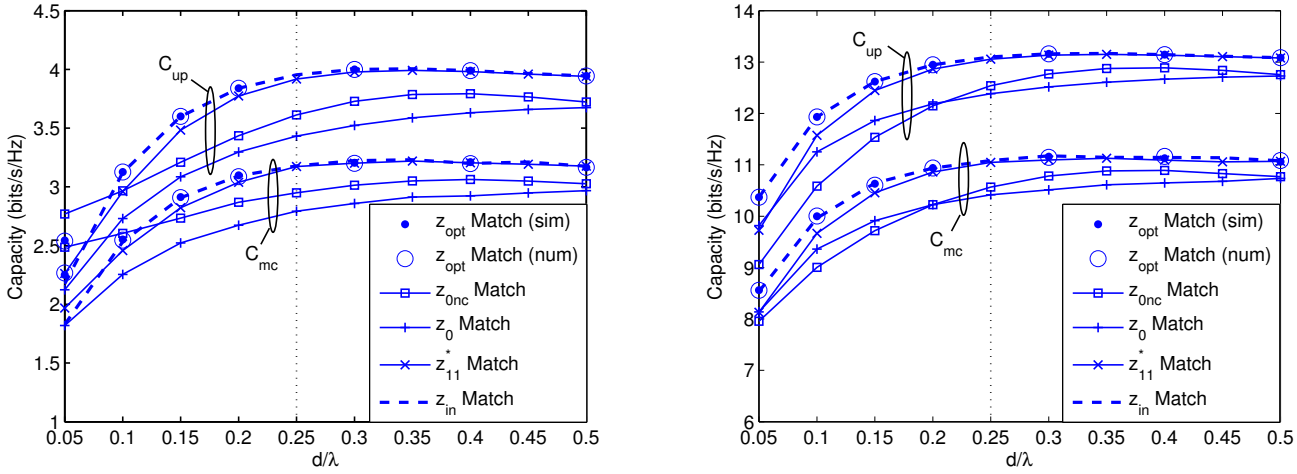

(a) $\rho_r = 5dB$ (b) $\rho_r = 20dB$

Fig. 5. The mean capacity and upper bound capacity with various matching networks as a function of d with different ρ_r.

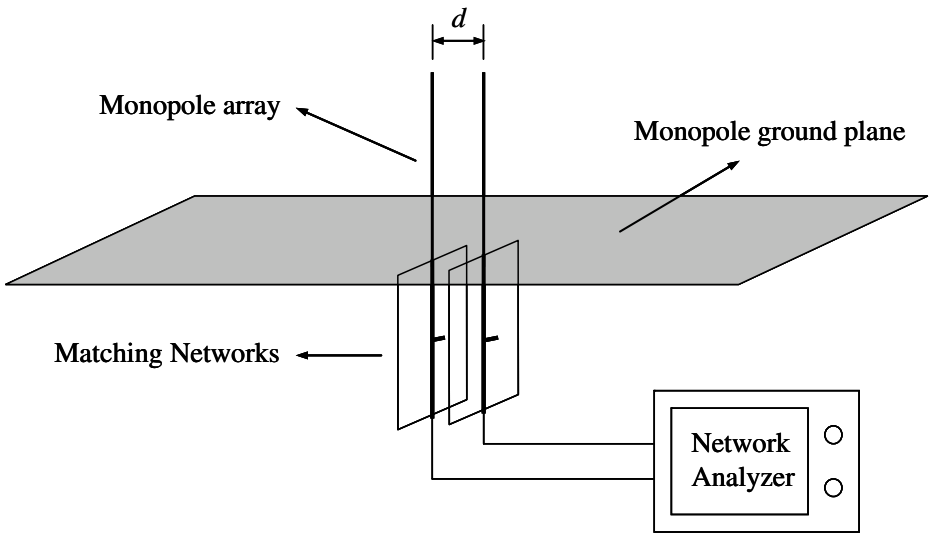

Fig. 6. Experimental setup of two $\lambda/4$ monopoles mounted on a ground plane and connected to matching networks.

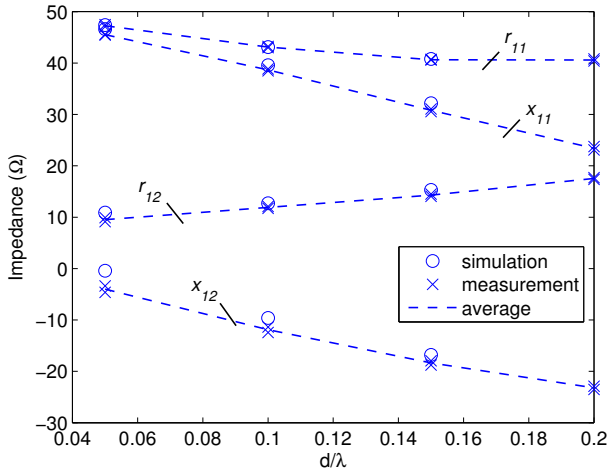

Fig. 7. Simulation and measured results of the self and mutual impedances for a two-$\lambda/4$-monopole array with various antenna spacings.

TABLE II

COMPARISON OF THE ERGODIC CAPACITY BETWEEN CHOSEN LOADS WITH ANTENNA PARAMETERS FROM SIMULATION AND MEASUREMENT & CONTRAST BETWEEN NUMERICAL AND SIMULATION RESULTS OF OPTIMUM SINGLE-PORT IMPEDANCE.

	$Impedances\ (\Omega)$	$C_m\ (bits/s/Hz)$	
		sim†	mea‡
z_A	70.69 - j9	7.8572	8.4699
z_B	1.5 - j12.8	7.8150	8.3154
z_C	4.06 + j3	5.6516	6.2921
z_D	16.5 - j12	8.4068	9.1431
z_0	50	7.9810	8.6913
z_{11}^*	45.6 - j20.5 (sim)	8.0201	/
	45.5 - j19.22 (mea)	/	8.7579
z_{in}	8.29 - j11.46 (sim)	8.4517	/
	11.41 - j11.88 (mea)	/	9.2046
z_{opt}	8.67 - j11.85 (sim)	8.5313	/
	11.23 - j11.6 (mea)	/	9.2688
z_{opt}^n	9.09 - j11.46 (sim)	8.4558	/
	11.23 - j11.89 (mea)	/	9.2353

†results based on antenna parameters in simulation
‡results based on antenna parameters in measurement
^{n}numerical results